

Imaging heterogeneities with electrical impedance tomography: laboratory results

*Original*

Imaging heterogeneities with electrical impedance tomography: laboratory results / A., Borsic; Comina, Cesare; Foti, Sebastiano; Lancellotta, Renato; Musso, Guido. - In: GEOTECHNIQUE. - ISSN 0016-8505. - STAMPA. - 55:7(2005), pp. 539-547. [10.1680/geot.2005.55.7.539]

*Availability:*

This version is available at: 11583/1507642 since:

*Publisher:*

ICE

*Published*

DOI:10.1680/geot.2005.55.7.539

*Terms of use:*

This article is made available under terms and conditions as specified in the corresponding bibliographic description in the repository

*Publisher copyright*

(Article begins on next page)

## Imaging heterogeneities with electrical impedance tomography: laboratory results

A. BORSIC\*, C. COMINA†, S. FOTI‡, R. LANCELOTTA† and G. MUSSO‡

**Electrical impedance tomography (EIT) is commonly used on site as a characterisation and monitoring tool. In the present work this technique has been applied at laboratory scale in order to investigate its capabilities in controlled conditions, with particular reference to the detection of anomalies in sandy samples. Various configurations have been studied, investigating heterogeneities due to variation of porosity, grain size distribution and clay content. The results show the great potential of EIT as an imaging tool in laboratory equipment to check sample homogeneity and to monitor processes during tests.**

**KEYWORDS:** erosion; fabric/structure of soils; geophysics; laboratory tests; sands

**La tomographie d'impédance électrique (EIT) est utilisée couramment sur le terrain comme outil de caractérisation et de contrôle. Dans cet exposé, nous appliquons cette technique en laboratoire pour étudier ses capacités dans des conditions contrôlées, en étudiant plus particulièrement la détection d'anomalies dans des échantillons de sable. Nous étudions diverses configurations en recherchant les hétérogénéités dues à une variation de la porosité, de la distribution des dimensions de grains et au contenu argileux. Les résultats montrent le fort potentiel d'EIT en tant qu'outil d'imagerie en laboratoire pour vérifier l'homogénéité des échantillons et contrôler les processus pendant les essais.**

### INTRODUCTION

The electric impedance tomography (EIT) technique is of common application in geophysical investigations, thanks to its capability of imaging the electric conductivity distribution of the investigated formations, and hence detecting the presence of heterogeneities (Reynolds, 1997).

Applications of EIT also include investigating pore fluid properties, and in this respect it is often used to monitor the flow of contaminants, providing information on their spatial scattering and on location of contamination sources (Ogilvy *et al.*, 2002; Binley & Daily, 2004). In petroleum engineering the hydrocarbon content of oil-carrying formations is commonly estimated on the basis of conductivity measurements performed by means of the EIT technique. Attempts to relate measured conductivity values to soil parameters such as porosity, degree of saturation and hydraulic conductivity can also be found in the literature (Abu-Hassanein *et al.*, 1996). As the electrical conductivity of soils is a function of several variables, *in situ* measurements often lead to qualitative information, and need to be cross-checked with other data in order to originate quantitative analyses.

Because of the control exerted on boundary and initial conditions, laboratory tests can be used as a counterpart of site geophysical tests in order to improve their interpretation. In the present study the potential of EIT as an imaging tool in laboratory equipment is assessed, as well in the perspective of checking sample homogeneity and monitoring non-stationary processes (e.g. infiltration, diffusion, chemical reactions, porosity variations, strain localisation and saturation-desaturation processes).

An application to monitoring of salt diffusion in fully saturated sandy samples is reported by Comina *et al.* (2005).

In order to investigate the ability of EIT in locating heterogeneities of different nature, tests have been conducted under controlled sample composition and boundary conditions. Anomalies of different nature have been created in samples, changing the composition or varying soil density. Both aspects are known in the literature to affect electrical conductivity, so that the test results can be interpreted in the framework of existing theories or empirical relationships (Mitchell, 1993; Yeung & Menon, 1997).

Indeed various formulae (e.g. Archie, 1942; Pfnankuch, 1969; Mitchell, 1993; Berryman, 1995) can be found in the literature relating the electrical conductivity of saturated soils to the physico-chemical properties of the mixture (concentration of ionic species, porosity, tortuosity, specific surface, cation exchange capacity). These relations are based on the fact that the solid phase is non-conductive, so that electrical charges travel only in the bulk fluid or along the double layer at the interface between the solid phase and the wetting solution (this latter phenomenon is known as surface conductance, and can be very relevant in the presence of clay fractions and low-concentration electrolyte).

In the paper, electrical tomography is first introduced with specific reference to the reconstruction technique adopted in the present work. Then the equipment used for the laboratory tests is described. Finally the results of a series of benchmark tests, specifically devised to explore the full potential of the technique, are reported. It is worthwhile to remark that, in the literature, results are often reported in terms of electrical resistivity rather than its inverse, electrical conductivity. In this work the latter is used as reference parameter, for consistency with the theoretical formulation of the problem.

### ELECTRICAL IMPEDANCE TOMOGRAPHY

EIT is a technique that allows estimation of the spatial distribution of the electrical conductivity within an object from impedance measurements at its boundary. Usually

Manuscript received 19 July 2004; revised manuscript accepted 6 June 2005.

Discussion on this paper closes 1 March 2006, for further details see p. ii.

\* SC-AIP s.a.s., c/o Incubatore Imprese Innovative del Politecnico di Torino, Italy.

† Department of Structural and Geotechnical Engineering, Politecnico di Torino, Italy.

‡ Department of Structural and Geotechnical Engineering, Politecnico di Torino, Italy. Currently with Geomechanical Group, Eni E&P Division, Italy.

several electrodes are applied to the surface of the object, and known currents are then imposed on some of them. The voltages resulting from the application of such currents are then measured on the remaining electrodes. As the collected measurements are linked to the object conductivity by known physical laws, it is possible to estimate from them the distribution of conductivity within the object. Such an estimation process is called tomographic reconstruction.

#### Forward model

The solution of the forward problem links the voltage measurements to the object conductivity. Assuming that the object under measurement has a conductivity that is linear and isotropic, and that the electric and magnetic fields are slowly varying, the electric potential  $u$  inside the body  $\Omega$  is governed by the stationary form of Maxwell's equations:

$$\nabla(\sigma \nabla u) = 0 \quad (1)$$

where  $\sigma$  is the electrical conductivity of the imaged body. The presence of the electrodes is taken into account via appropriate boundary conditions. One model for electrodes, which provides accurate predictions at least for laboratory experiments (Borsic, 2002), is the complete electrode model proposed by Somersalo *et al.* (1992). The model assumes that electrodes are good conductors and therefore that the electric potential of each electrode is constant over its entire surface. Moreover, the model assumes that there is contact impedance at the interface between the electrode and the object under measurement. Under these assumptions, the following relation holds for each electrode,  $l = 1 \dots L$ :

$$V_l = u + z_l \sigma \frac{\partial u}{\partial \vec{n}} \quad \text{on } \partial\Omega_l, \quad l = 1, \dots, L \quad (2)$$

where  $V_l$  is the potential of the  $l$ th electrode,  $z_l$  is the contact impedance of the  $l$ th electrode,  $u$  and  $\sigma$  are the object potential and conductivity,  $\vec{n}$  is the outwards normal to  $\partial\Omega$ , and  $\partial\Omega_l$  is the portion of  $\partial\Omega$  underneath electrode  $l$ .

Stimuli are accounted for by specifying for each electrode that

$$\int \sigma \frac{\partial u}{\partial \vec{n}} = I_l \quad \text{on } \partial\Omega_l, \quad l = 1, \dots, L \quad (3)$$

where  $I_l$  is the current injected into the  $l$ th electrode. Equations (2) and (3) apply to the portions of  $\partial\Omega$  that falls underneath each electrode. To the remaining parts of  $\partial\Omega$  (inter-electrode gaps), the following relationship applies:

$$\sigma \frac{\partial u}{\partial \vec{n}} = 0 \quad (4)$$

as no current density is crossing the free surface of the object under measurement. Equations (2)–(4) specify the model for the electrode; voltages on the electrodes are, however, specified to within an arbitrary additive constant, as no reference potential has been specified. As this is an arbitrary choice, usually the model is complemented with the additional condition

$$\sum_{l=1}^L V_l = 0 \quad (5)$$

which allows the unique determination of all  $V_l$ .

#### Reconstruction

The inverse operator, which given the measurements would return the conductivity, is not known in the general case. Hence reconstruction algorithms make use of a forward model, and the reconstruction is formulated as a non-linear

least-squares problem, where the conductivity of the forward model is varied until a satisfactory match between the measurements simulated by the forward model and the real measurements is met. Most reconstruction codes implement the forward model with a finite element solver (Paulson *et al.*, 1992; Vauhkonen, 1997; Borsic, 2002; Polydorides & Lionheart, 2002), discretising both domain  $\Omega$  and the conductivity distribution. The reconstruction problem is therefore stated as

$$\mathbf{s}_{\text{rec}} = \arg \min \|h(\mathbf{s}) - \mathbf{v}\|_2^2 \quad (6)$$

where  $\mathbf{v}$  is the vector of measured voltages,  $\mathbf{s}$  is the discrete conductivity,  $h$  is the non-linear forward operator from model space to measurements space, and  $\|\dots\|_2^2$  indicates the squared 2-norm. The reconstruction problem, both in its continuous form and in its discrete form expressed by equation (6), is *ill posed* in the sense that small perturbations in the measured data can cause arbitrarily large errors in the estimated conductivity (Calderon, 1980; Sylvester & Uhlman, 1987). Given the ill-posedness of the inverse problem, reconstruction algorithms adopt regularisation techniques, in order to obtain a stable solution. In practical terms, such ill-conditioning arises from certain patterns of conductivity for which the corresponding measurements are extremely small (Breckon, 1990; Borsic, 2002), and which are therefore affected by measurement noise.

Such patterns of conductivity, for which the observations are unreliable, corrupt the reconstruction. Regularisation techniques are adopted in order to prevent such problems. Commonly equation (6) is solved using the Tikhonov regularisation, formulating the reconstruction as

$$\mathbf{s}_{\text{rec}} = \arg \min \|h(\mathbf{s}) - \mathbf{v}\|_2^2 + \alpha F(\mathbf{s}) \quad (7)$$

where  $F(\mathbf{s}) \geq 0$  is the regularisation function, and  $\alpha$  is a positive scalar called the Tikhonov factor. Specifically  $F$  acts as a penalty term, by taking large values corresponding to distributions  $\mathbf{s}$  that are to be prevented in the reconstructed profile. The effect of  $F$  on the reconstructions can be adjusted by varying the value of  $\alpha$ . As the conductivity is discrete, the regularisation function is usually expressed as  $F(\mathbf{s}) = \|\mathbf{L}\mathbf{s}\|_2^2$ , where  $\mathbf{L}$  is the regularisation matrix. The reconstruction is therefore formulated as

$$\mathbf{s}_{\text{rec}} = \arg \min \|h(\mathbf{s}) - \mathbf{v}\|_2^2 + \alpha \|\mathbf{L}\mathbf{s}\|_2^2. \quad (8)$$

As anticipated, the role of the regularisation function is to penalise the presence in the reconstructed image of conductivity distributions for which observations are exceedingly small compared with the noise in the measurements. Thorough discussions on the choice of  $\alpha$  and on regularisation techniques in EIT can be found in Kolehmainen (2001) and Borsic *et al.* (2002). The classical choice for the matrix  $\mathbf{L}$  is the identity matrix. A similar choice is made in the NOSER algorithm (Cheney *et al.*, 1990), which uses a positive diagonal matrix. Matrices that approximate first- and second-order differential operators have also been proposed (Hua *et al.*, 1988). All these regularisation methods achieve the stability of the inversion by penalising sudden variations in the conductivity, and hence offering a trade-off between stability of the reconstruction and sharpness of image.

#### EXPERIMENTAL SET-UP

Experiments have been performed on a cylindrical Perspex cell, with internal diameter of 130 mm and height of 100 mm (Comina, 2005). Sixteen electrodes (thin silver plates, 5 mm  $\times$  80 mm  $\times$  0.1 mm) are applied on the lateral surface of the soil sample with constant spacing (see Fig. 1).



Fig. 1. Measurement set-up: 1, personal computer; 2, data acquisition system; 3, inverter; 4, measuring cell

The shape and position of the electrodes have been chosen in order to realistically reproduce a 2D propagation of electric currents inside the sample. The decision to use 16 electrodes is a compromise between simplicity of design and resolution. In EIT the resolution is determined by the number of electrodes and by the signal-to-noise ratio of the measurements. Industrial and medical applications of EIT on round or 'almost round' objects show that the use of 32 electrodes only marginally improves the resolution over the 16-electrode configuration (Holder, 2004).

Electrodes are connected to the data acquisition system using silver wires, welded to their back and protruding outside the cell through thin holes (1 mm in diameter). A silicon injection in these holes avoids leakage of the interstitial fluid from the cell. For the same reason, the base of the cell is equipped with an O-ring, providing a watertight contact.

The data acquisition system is the Complex Impedance Tomograph (CIT) mark I, a prototype designed by Iridium Italia s.a.s. in collaboration with the Applied Geophysics Section of Politecnico di Torino (Sambuelli *et al.*, 2002). The main characteristics of the instrument are reported in Table 1. The instrument is a single current source tomograph.

A digital direct synthesiser is used for the generation of the a.c. waveform, which is then fed to a voltage-controlled current source and applied via a multiplexer to the pair of driving electrodes. The output impedance of the current source is estimated to be in the range of 200 M $\Omega$ , making it possible to drive currents in very resistive media. The injected current intensity is measured on a shunt resistor in series with the driving pair, which ensures accurate measurement of the applied current. A second multiplexer connects the electrodes to an analogue to digital converter for voltage measurement. The output signals are processed by an on-board digital signal processor, which separates in-phase and out-of-phase components (Bena, 2003). The instrument is

controlled by a PC to implement the measurement scheme and to gather the results.

The experimental data have been collected using the 'opposite' measurement protocol (Hua *et al.*, 1988; Lionheart *et al.*, 2001), in which currents are injected by diametrical electrodes and potential differences are measured for all possible pairs of the remaining electrodes. Switching the input pair, 96 linearly independent measurements can be collected over the 16 electrodes of the cell. This protocol is preferred to the adjacent measurement method because it offers a better resolution, as the current travels with greater uniformity inside the sample (Lionheart *et al.*, 2001).

Tomographic inversions have been performed with a commercial EIT toolbox (SC-AIP, 2004). The reconstruction is formulated as in equation (8), and the forward model is a finite element implementation of equations (1)–(5). The cell layout and the sample geometry are such that a 2D model can be used. The regularisation matrix  $L$  of equation (8) is chosen to be a discrete representation of the Laplacian. The toolbox uses a double mesh: a coarse mesh is used to represent the discrete conductivity, and a second, finer mesh is used to represent the electric potential. The number of elements of the coarse mesh coincides with the number of unknowns of the reconstruction process: hence it has to be chosen with care, considering the number of available measurements in the light of sensitivity and non-uniqueness issues. For the interpretation of the tests reported in the present paper, the triangular elements in the coarse mesh (degrees of freedom of the conductivity) are 812, and the mesh is illustrated in Fig. 2. As such a mesh is not appropriate for an accurate solution of the forward problem, a second and finer mesh is used for the computation of simulated voltages at the electrodes. The fine mesh, shown in Fig. 3, is obtained by adaptive refinement of the coarse mesh. The forward solver projects the conductivity  $s$  from the coarse mesh to the fine one each time a forward solution is needed, and the FEM stiffness matrix is assembled for the fine mesh. The refinement of the mesh allows a good accuracy in the approximation of the electric potential, especially in proximity of the electrodes, where it varies rapidly owing to the injected currents (Vauhkonen, 1997; Borsic, 2002).

Table 1. Characteristics of the complex impedance tomograph (Bena, 2003)

Maximum output current: A	0.25
Maximum output voltage: V	40
Operative frequencies	12 steps from 0.488 to 976 Hz
Acquisition channels	16
Resolution on phase angles: mrad	$\approx 1$
Resolution on voltage: $\mu V$	100
Resolution on current: $\mu A$	10
Input impedance: M $\Omega$	200

## EXPERIMENTAL RESULTS

A testing programme has been carried out to evaluate the capabilities of laboratory EIT by setting some benchmark problems: presence of inclusions, variation of density inside



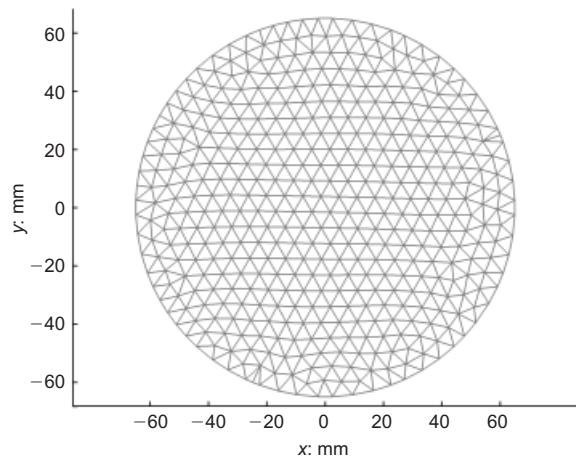


Fig. 2. Coarse finite element mesh

the sample and variation of grain size distribution. All the above problems have been studied using reconstituted samples saturated with tap water, in order to allow conduction in sandy materials. Indeed, as the testing programme has been pursued in clean quartz sands, where no surface conductance is expected, electrical conduction relied on the migration of dissolved ions, and therefore the use of distilled water would have led to exceptionally high resistive samples (Mualen & Friedman, 1991).

#### Calibration

Preliminary tests have been performed to check the reliability of the reconstruction process by imaging uniform samples of known conductivity. The cell was filled with water solutions having different concentrations of NaCl. As an example, Fig. 4 shows the reconstruction for a 0.1 mol solution. Excluding the small deviations in the proximity of the electrodes, the reconstruction gives a uniform conductivity distribution with a coefficient of variation of about 3% and a mean value of 10.55 mS/cm. This reconstructed value matches very well the theoretical conductivity for this solution (10.53 mS/cm), which has been double-checked with an independent measurement by using an electrical conductimeter.

Similar results have been obtained for other salt concen-

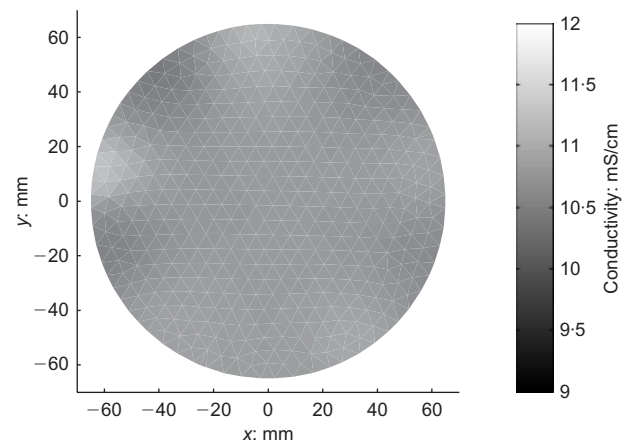


Fig. 4. EIT reconstruction of a NaCl 0.1 mol water solution

trations. These tests confirmed the adequacy of the reconstruction process for the specific experimental set-up, especially as far as the double mesh is concerned. Moreover, they showed that accurate prediction of the conductivity is possible.

#### Inclusions

The investigated heterogeneities were more conductive inclusions in a clean sand sample. As surface conductance is a significant factor affecting the conductivity of samples in the presence of a clay fraction (Bussian, 1983), the inclusions have been created by adding different percentages of clay to Ticino sand. Fig. 5(a) represent a sample in which two cylinders of Ticino sand, 38 mm in diameter, mixed with 10% in weight of Monastero Bormida clay are embedded in a sample of clean Ticino sand. As shown in Fig. 5(b), the reconstructed conductivity is reliable both in locating the two heterogeneities and in detecting their dimensions. It is worthwhile to recall that, because of the regularisation techniques adopted in the solution of the inverse problem (see subsection 'Reconstruction' above), the final solution is a smooth representation, whereas the problem is characterised by sharp boundaries. Hence it is not possible to quantify exactly the difference between the actual size of the inclusions and their size in the recon-

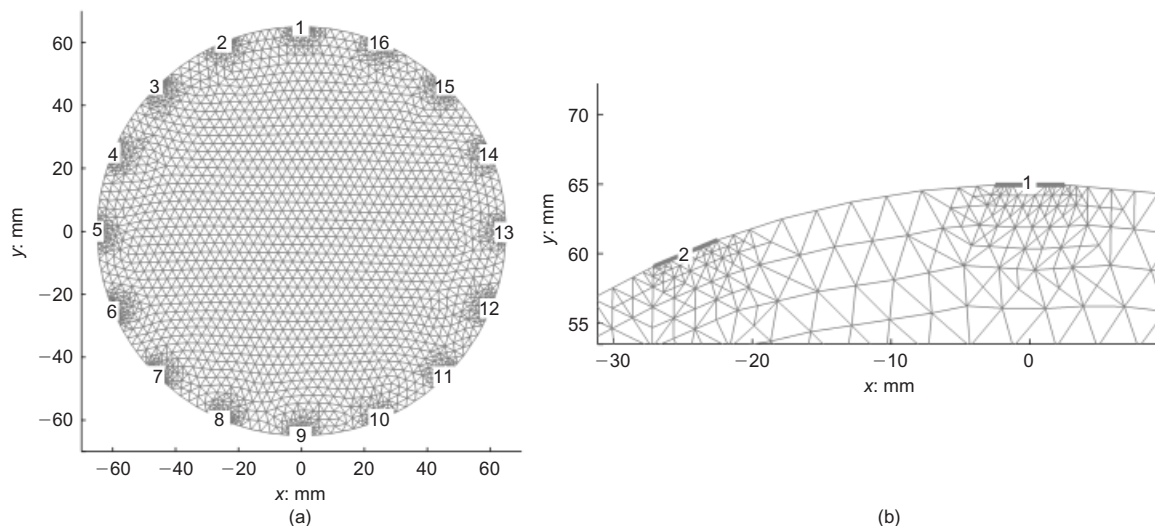


Fig. 3. Fine finite element mesh: (a) global view; (b) close-up view near electrodes 1 and 2

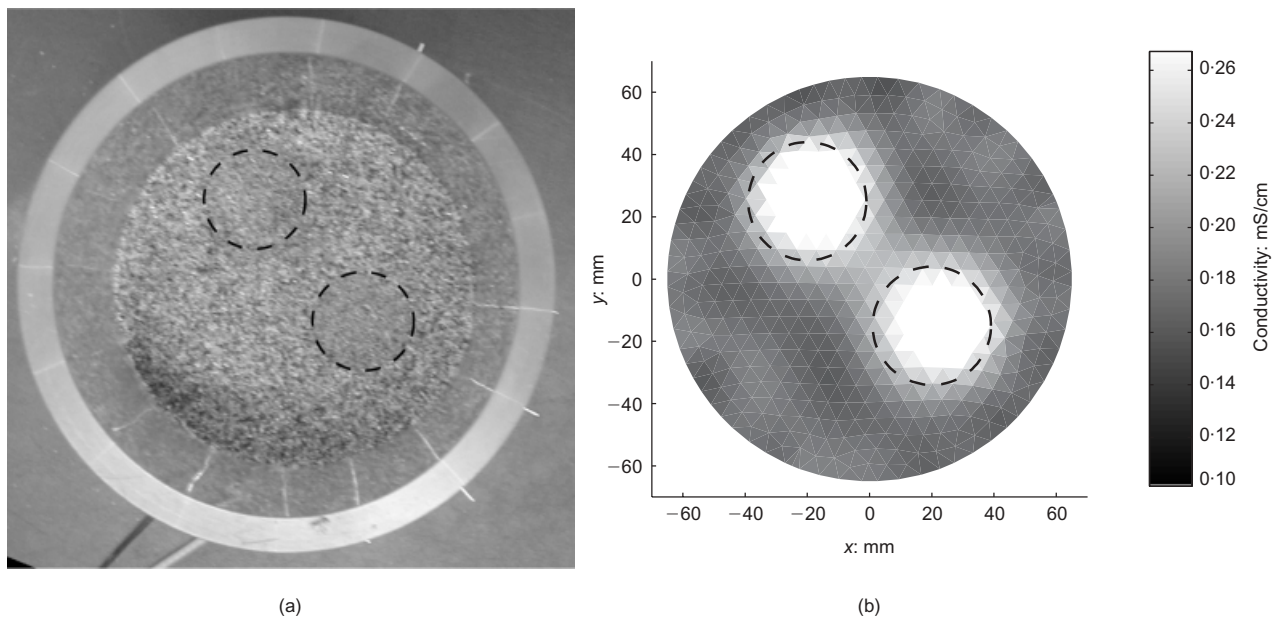


Fig. 5. (a) Sample with cylindrical inclusions of Ticino sand mixed with 10% in weight of clay; (b) EIT reconstruction

structed image. Nevertheless, if a given threshold of conductivity is chosen in the reconstructed image, the position of the inclusions can be estimated. For example, considering in the present test the elements in the mesh having conductivity higher than 0.25 mS/cm, the position of the inclusions is estimated with an error below 0.05 rad (respectively 0.032 rad for the upper inclusion and 0.047 rad for the lower inclusion).

Similar tests have been performed considering inclusions less conductive than the surrounding sample, and good performance has also been shown in those cases (Comina *et al.*, 2005).

#### Density variations

In order to obtain zones of different density, a sample was prepared by placing Ticino sand around a cylindrical stainless steel sampler (38 mm in diameter), later removed to let

the sand collapse and fill the hole (Fig. 6(a)). This zone of looser material is well detected in the reconstructed image (Fig. 6(b)), as its higher porosity corresponds to higher conductivity. In this case the transition from the relaxed zone to the denser one is smooth, and therefore more suitable to be properly detected by the reconstruction algorithm. Although a quantitative assessment has not been attempted in this case, the correspondence between the looser, more conductive material and the position of the original void (dashed circle) is quite clear in Fig. 6(b). As in this case the observed differences in conductivity are very small, their evaluation is an index of the remarkable quality of the experimental data.

A significant case of localised variations of porosity is associated with strain localisation in shearing of dense sands. In order to assess the potential of EIT in monitoring shear band formation, a synthetic example of reconstruction was first studied.

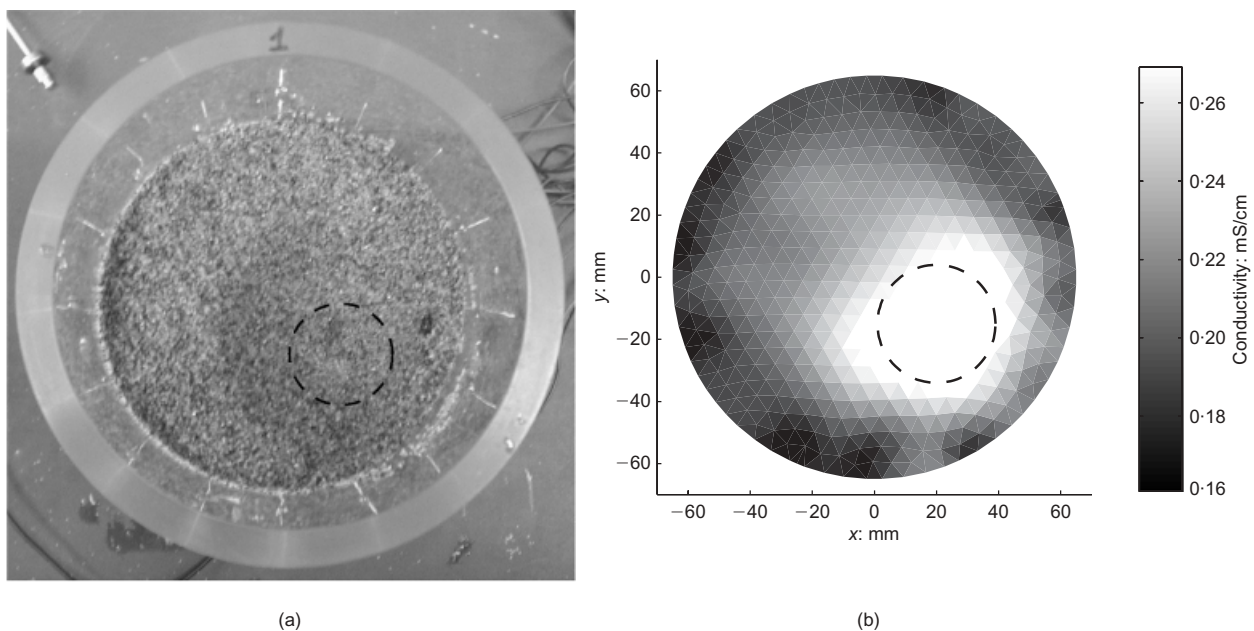


Fig. 6. (a) Looser zone inside a dense sand sample; (b) EIT reconstruction

In granular materials, such as the Ticino sand adopted for our experimental tests, the thickness of a shear band is typically about 10–20 times the mean diameter of the sand grains (Mühlhaus & Vardoulakis, 1987), whereas variations of porosity are not easily determined but are always related to a porosity increase inside the band (Desrues *et al.*, 1996). Assuming the properties of Ticino sand, a synthetic model of conductivity has been constructed simulating the presence of a shear band of about 5 mm thickness with a variation of porosity equal to 1% with respect to the surrounding material (Fig. 7(a)). The conductivity values for the model have been derived using Bruggeman's formula (see next section). Using this model, synthetic readings at the electrodes have been obtained with the forward solver. These data have been perturbed with Gaussian noise (1%) to reproduce experimental errors, and used for the reconstruction process (Fig. 7(b)). Synthetic results show that the experimental set-up and the inversion algorithm are in principle suitable for studying shear banding in dense sands, and hence EIT can be an alternative to more expensive techniques such as radiographic and microscopic observations (Nemat-Nasser

& Okada, 2001) or X-ray computed tomography methods (Desrues *et al.*, 1996).

Considering that a shear band cannot be realistically produced in the cell used in the present study, a thin, band-shaped looser zone was created by extracting a 2 mm metal sheet placed in the cell before preparation of the sample (Fig. 8(a)). Although the induced feature is very thin with respect to the overall dimensions, the reconstructed image is quite successful in detecting its presence and its orientation (Fig. 8(b)).

#### Grain size variations

Internal erosion is an important aspect in many geotechnical applications. In order to assess the capability of EIT to detect zones interested by internal erosion, a band of gap-graded material (Fig. 9) with thickness 4 mm was created in a uniform sand sample (Fig. 10(a)). The reconstructed image (Fig. 10(b)) shows that the band-shaped inclusion is detected reasonably well as a more resistive zone, because the change

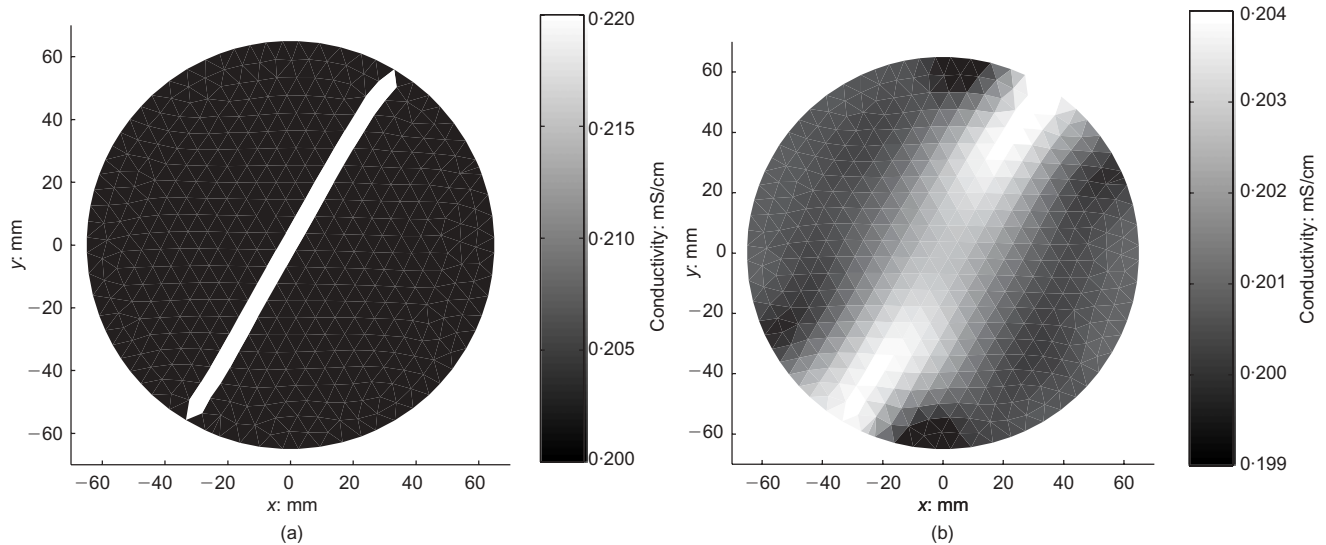


Fig. 7. (a) Synthetic conductivity model of a shear band; (b) EIT reconstruction

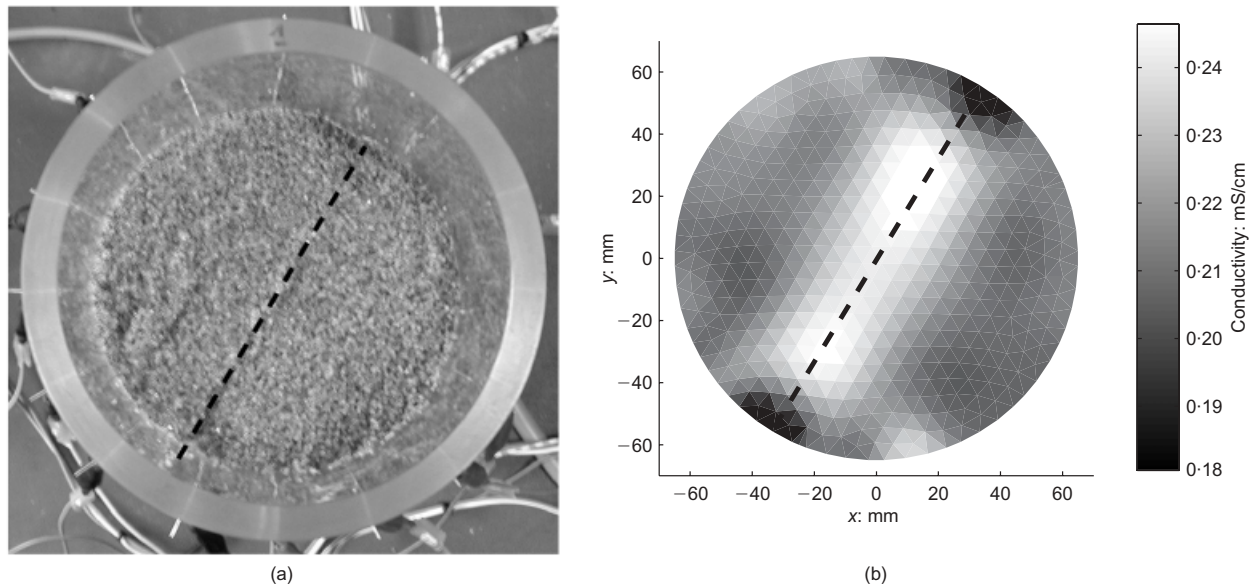


Fig. 8. (a) Band-shaped inclusion of loose sand; (b) EIT reconstruction



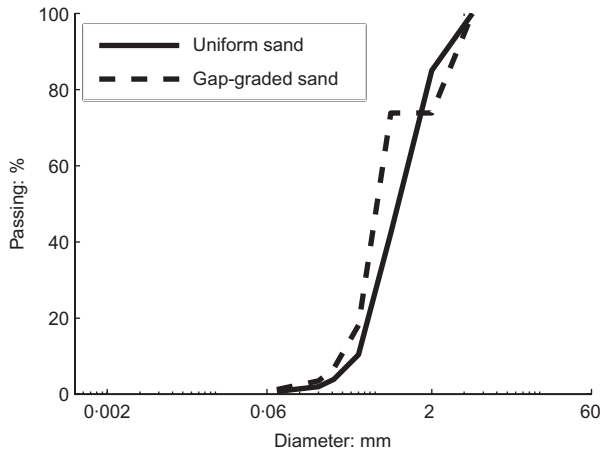


Fig. 9. Grain size distribution of uniform and gap-graded sands

in grain size distribution affects porosity and fabric, giving more tortuous paths for free ions.

#### ESTIMATING POROSITY

Several attempts can be found in the literature to relate the electrical conductivity of a soil to its porosity  $n$  on the basis of the electrical conductivity of its constituents (Berryman, 1995). One of the most used relationships is Archie's formula (Archie, 1942), which in the case of brine-saturated sand samples can be expressed as

$$\frac{\sigma_w}{\sigma^*} = \frac{a}{n^m} \quad (9)$$

where  $\sigma^*$  is the soil conductivity,  $\sigma_w$  is the conductivity of the interstitial water,  $m$  is an empirical factor related to the degree of cementation, and  $a$  is an indicator of the tortuosity. Archie's formula is purely empirical, and has been recognised as an oversimplification. Nevertheless, it can still lead to acceptable results whenever no surface conductance is occurring.

Bruggeman (1935) proposed a theoretical formulation based on the so-called differential effective medium approach. The relationship between porosity  $n$ , the conductivity

of the soil ( $\sigma^*(n)$ ) and the conductivity of the fluid phase ( $\sigma_w$ ) is expressed by the differential equation

$$(1 - n) \frac{d}{dn} \sigma^*(n) = \frac{\sigma_w - \sigma^*(n)}{\sigma_w + 2\sigma^*(n)} 3\sigma^*(n) \quad (10)$$

By integrating equation (10) with the condition  $\sigma^*(n) = \sigma_s$  for  $n = 0$ , where  $\sigma_s$  is the conductivity of the solid phase, it is then found that

$$n = \frac{\sigma_s - \sigma^*}{\sigma_s - \sigma_w} \cdot \left( \frac{\sigma_w}{\sigma^*} \right)^{1/3} \quad (11)$$

Under the assumption of infinite resistivity for sand grains ( $\sigma_s = 0$ ), equation (11) simplifies to  $n = (\sigma^*/\sigma_w)^{2/3}$ .

The reliability of Bruggeman's formula has been verified by testing three uniform Ticino sand samples of known porosity. The value of  $\sigma_w$  was obtained from independent measurements performed with a conductimeter on a sample of pore water. The average normalised conductivity inside each sample and the associated standard deviation are reported in Fig. 11.

Finally, Fig. 12(b) shows the EIT reconstruction of a saturated sample of air-pluviated Ticino sand with a cylindrical inclusion (diameter 38 mm) of compacted sand (Fig. 12(a)). The reconstructed image locates in a reliable manner the denser

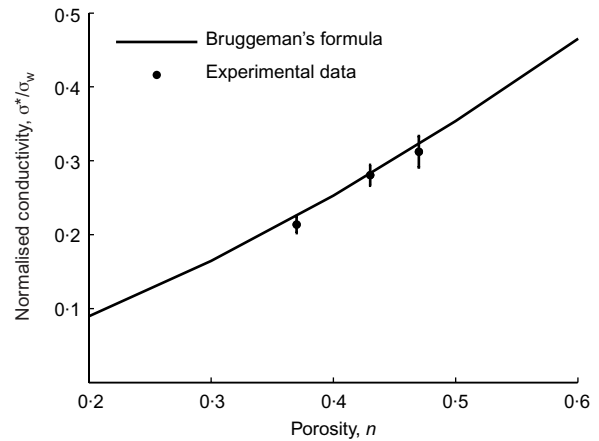
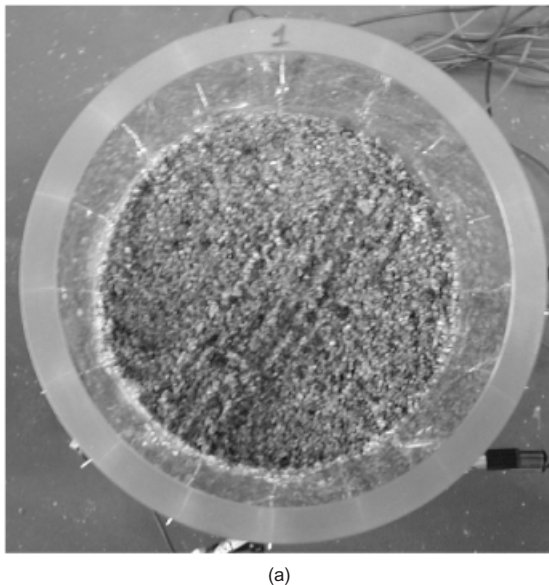
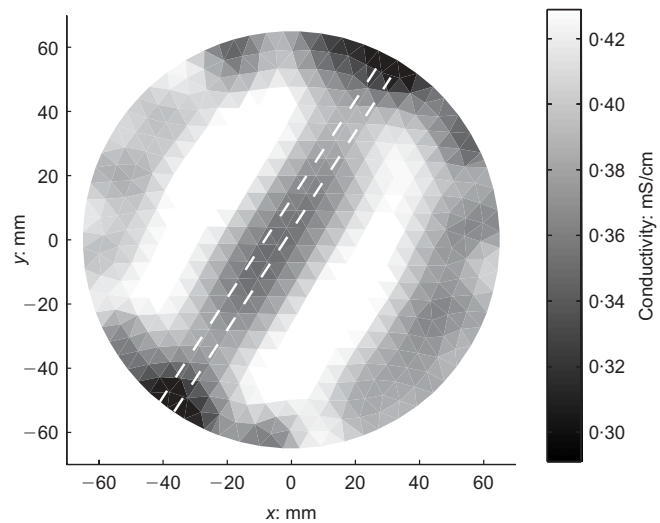


Fig. 11. Validation of Bruggeman's formula using EIT data



(a)



(b)

Fig. 10. (a) Inclusion of a band-shaped zone (thickness 4 mm) of gap-graded sand within a sample of uniform sand; (b) EIT reconstruction



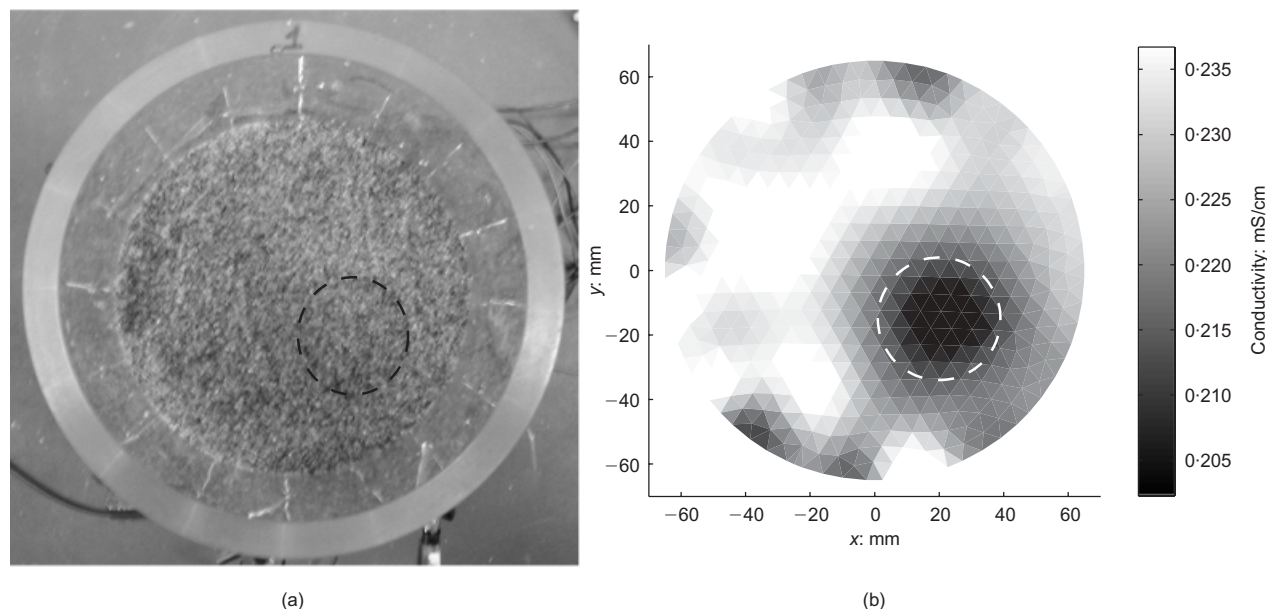


Fig. 12. (a) Cylindrical inclusion of compacted sand within a loose sand sample; (b) EIT reconstruction

(less conductive) zone. The porosity values obtained with equation (11) using the average conductivity for each zone (Table 2) are in reasonable agreement with those measured with the conventional procedure (Table 3), proving the potential of the technique for quantitative indirect estimation of soil properties.

## CONCLUSIONS

The work presented in this paper was aimed at evaluating the use of electric impedance tomography for the detection and characterisation of heterogeneities in sand samples. Non-homogeneous soil samples were artificially created and EIT reconstructions performed at the laboratory scale. Results proved that this technique can satisfactorily detect anomalies of interest for many geotechnical engineering applications, so that its development for laboratory tests appears promising.

Inclusions of different shapes due to local changes in density were also detected quite accurately in the presence of reduced differences in soil conductivity. Accuracy proved to be satisfactory in the case of both less conductive and more conductive inclusions. Moreover, the quantitative assessment of porosity in non-homogeneous samples, per-

formed on the basis of sound theoretical relationships, leads to very satisfying results.

The detection of thin, looser bands indicates that valuable information could be gained during tests where mechanically induced localisation (e.g. shear banding) is occurring. Moreover, the possibility of recognising gap-graded materials in a uniform matrix shows the potential in the study of erosion phenomena.

Further ongoing developments include the study of processes related to coupled chemo-mechanical phenomena and to changes in the degree of saturation. In the former case, changes in the electrical conductivity will be interpreted in terms of changes in the bulk ionic concentration and related to strains occurring in the soil. The latter technique, calibrated on the basis of extended formulations of Archie's law, could help in local evaluations of the degree of saturation during transient processes.

## ACKNOWLEDGEMENTS

The authors are indebted to Professor Luigi Sambuelli (DITAG, Politecnico di Torino) for constructive discussions on the topic, and for the possibility of using the CIT. The authors are also grateful to Professor J. C. Santamarina (Georgia Institute of Technology, Atlanta, USA) for valuable suggestions.

Table 2. Porosity values from EIT reconstruction using Brugge-man's formula

	Sample	Inclusion
Water conductivity, $\sigma_w$ : mS/cm	0.765	
Soil conductivity, $\sigma^*$ : mS/cm	$0.240 \pm 3.2\%$	$0.205 \pm 2.9\%$
Porosity $n$	$0.46 \pm 2.2\%$	$0.42 \pm 1.9\%$

Table 3. Measured porosity values

	Sample	Inclusion
Grain specific density, $G_s$	2.68	
Saturated specific weight, $\gamma$ : kN/m <sup>3</sup>	14.0	15.4
Porosity, $n$	0.48	0.43

## NOTATION

$a$	empirical factor in Archie's law
$F(s)$	regularisation function
$h$	non-linear forward operator from model space to measurements space
$I$	current
$L$	regularisation matrix
$m$	empirical factor in Archie's Law
$\vec{n}$	outwards normal to $\partial\Omega$
$n$	soil porosity
$s$	discrete conductivity
$s_{rec}$	reconstructed discrete conductivity
$u$	electric potential of continuous body
$V$	electrical potential of electrode
$v$	measured voltages
$z$	contact impedance of electrode
$\alpha$	Tikhonov factor

- $\sigma$  electrical conductivity  
 $\sigma^*$  electrical conductivity of porous medium  
 $\sigma_s$  electrical conductivity of solid grains  
 $\sigma_w$  interstitial water electrical conductivity  
 $\partial\Omega$  boundary surface for body  $\Omega$   
 $\Omega$  continuous body  
 $\|\dots\|_2^2$  squared 2-norm

## REFERENCES

- Abu-Hassanein, Z. S., Benson, C. H. & Blotz L. R. (1996). Electrical resistivity of compacted clays. *J. Geotech. Engng* **122**, No. 5, 397–406.
- Archie, G. E. (1942). The electrical resistivity log as an aid to determining some reservoir characteristics. *Trans. AIME* **146**, 54–63.
- Bena, E. (2003). *Tomografia elettrica di impedenza per la stima della quantità di solido in miscela bifase liquido-solido*. Masters thesis, Politecnico di Torino (in Italian).
- Berryman, J. G. (1995). Mixture theories for rock properties. In *A handbook of physical constants*, pp. 205–228. Washington, DC: American Geophysical Union.
- Binley, A. & Daily, W. (2004). The performance of electrical methods for assessing the integrity of geomembrane liners in landfill caps and waste storage ponds. *J. Environ. Engng Geophys.* **8**, No. 4, 227–237.
- Borsic, A. (2002). *Regularization methods for imaging from electrical measurements*. PhD thesis, School of Engineering, Oxford Brookes University.
- Borsic, A., Lionheart, W. R. B. & McLeod, C. N. (2002). Generation of anisotropic-smoothness regularisation filters for EIT. *IEEE Trans. Med. Img.*, **21**, No. 6, 579–587.
- Breckon, W. R. (1990). *Image reconstruction in electrical impedance tomography*. PhD thesis, Oxford Brookes Polytechnic.
- Bruggeman, D. A. G. (1935). Berechnung verschiedener physikalischer konstanten von heterogenen substanten. *Ann. Phys.* **24**, 636–679.
- Bussian, A. E. (1983). Electrical conductance in a porous medium. *Geophysics* **48**, No. 9, 1258–1268.
- Calderon, A. P. (1980). *On an inverse boundary problem*. Seminar on numerical analysis and its applications to continuum physics (eds W. H. Meyer and M. A. Raupp), pp. 65–73. Rio de Janeiro: Brazilian Math. Society.
- Cheney, M., Isaacson, D., Newell, J. C., Simake, S. & Goble, J. (1990). NOSER: an algorithm for solving the inverse conductivity problem. *Int. J. Imag. Sys. Technol.* **2**, No. 1, 66–75.
- Comina, C. (2005). *Imaging heterogeneities and diffusion in sand samples: electric and seismic methods*. PhD thesis, Politecnico di Torino, Torino.
- Comina, C., Foti, S., Lancellotta, R., Musso, G. & Borsic, A. (2005). Imaging heterogeneities and diffusion in sand samples. *Proc. 11th Int. Conf. of LACMAG 2005, Torino* **2**, 27–34.
- Desrues, J., Chambon, R., Mokini, M. & Mazerolle F. (1996). Void ratio evolution inside shear bands in triaxial sand specimens studied by computed tomography. *Géotechnique* **46**, No. 3, 529–546.
- Holder, D. S. (2004). *Electrical impedance tomography: Methods, history and applications*. London: Institute of Physics.
- Hua, P., Webster, J. G. & Tompkins, W. J. (1988). A regularised electrical impedance tomography reconstruction algorithm. *Physiol. Meas.* **9**, No. 2, 137–141.
- Kolehmainen, V. (2001). *Novel approaches to image reconstruction in diffusion tomography*. PhD thesis, Department of Applied Physics, Kuopio University, Finland.
- Lionheart, W. R. B., Kaipio, J. & McLeod, C. N. (2001). Generalized optimal current patterns and electrical safety in EIT. *Physiol. Meas.* **22**, No. 1, 85–90.
- Mitchell, J. K. (1993). *Fundamentals of soil behavior*, 2nd edn. New York: John Wiley & Sons.
- Mualen, Y. & Friedman, P. (1991). Theoretical prediction of electrical conductivity in saturated and unsaturated soil. *Water Resour. Res.* **27**, No. 10, 2771–2777.
- Muhlhaus, H. B. & Vardoulakis, I. (1987). The thickness of shear bands in granular materials. *Géotechnique* **37**, No. 3, 271–283.
- Nemat-Nasser, S. & Okada, N. (2001). Radiographic and microscopic observation of shear bands in granular materials. *Géotechnique* **51**, No. 9, 753–765.
- Ogilvy, R., Meldrum, P., Chambers, J. & Williams G. (2002). The use of 3D electrical resistivity tomography to characterise waste and leachate distribution within a closed landfill, Thriplow, UK. *J. Environ. Engng Geophys.* **7**, No. 1, 11–18.
- Paulson, K., Breckon, W. & Pidcock, M. (1992). Electrode modelling in electrical impedance tomography. *SIAM J. Appl. Math.* **52**, No. 4, 1012–1022.
- Pfannkuch, H. O. (1969). On the correlation of electrical conductivity properties of porous systems with viscous flow transport coefficients. *Proc. IAHR 1st Int. Symp. Fundamentals of Transport Phenomena in Porous Media, Haifa*, 42–54.
- Polydorides, N. & Lionheart, W. R. B. (2002). A Matlab toolkit for three-dimensional electrical impedance tomography: a contribution to the Electrical Impedance and Diffuse Optical Reconstruction Software project. *Meas. Sci. Technol.* **13**, No. 12, 1871–1883.
- Reynolds, J. M. (1997). *An introduction to applied and environmental geophysics*. Chichester: John Wiley & Sons.
- Sambuelli, L., Lollino, G., Morelli, G., Socco, L.V. & Bidone, L. (2002). First experiments on solid transport estimation in river-flow by fast impedance tomography. *Proc. 8th EEGS-ES Meeting, Aveiro*, CD-ROM.
- SC-AIP (2004). *EIT software and manual*. www.sc-aip.com
- Somersalo, E., Cheney, M. & Isaacson, D. (1992). Existence and uniqueness for electrode models for electric current computed tomography. *SIAM J. Appl. Math.* **52**, No. 4, 1023–1040.
- Sylvester, J. & Uhlman, G. (1987). A global uniqueness theorem for an inverse boundary value problem. *Ann. Math.* **125**, 153–169.
- Vauhkonen, M. (1997). *Electrical impedance tomography and prior information*. PhD thesis, Department of Applied Physics, Kuopio University, Finland.
- Yeung, A. T. & Menon, R. M. (1997). Discussion: Electrokinetic remediation. II: Theoretical model. *J. Geotech. Geoenviron. Engng* **123**, No. 11, 1078–1081.